Elucidating the failure of the Ideal Adsorbed Solution Theory for CO_2 /H_2O mixture adsorption in CALF-20

Krishna, R.; van Baten, J.M.

DOI
10.1016/j.seppur.2024.128269

Publication date
2025

Document Version
Final published version

Published in
Separation and Purification Technology

Separation and Purification Technology 352 (2025) 128269

Contents lists available at ScienceDirect

Separation and Purification Technology

journal homepage: www.elsevier.com/locate/seppur

Elucidating the failure of the Ideal Adsorbed Solution Theory for CO_2/H_2O mixture adsorption in CALF-20

Rajamani Krishna*, Jasper M. van Baten

Van 't Hoff Institute for Molecular Sciences University of Amsterdam, Science Park 904, 1098 XH Amsterdam, the Netherlands

ARTICLE INFO

Editor: Z Bao

Keywords:
CO_2 capture
Thermodynamic non-idealities
Segregated adsorption
Hydrogen bonding
Activity coefficients
Transient breakthrough
Fixed bed adsorber

ABSTRACT

The use of CALF-20 for CO_2 capture from humid flue gases has attracted a vast amount of attention from both academia and industry. The focus of this article is on CO_2/H_2O mixture adsorption for which published experimental data demonstrate the severe limitations of the Ideal Adsorbed Solution Theory (IAST) in providing a quantitative estimation of the component loadings. We use Configurational-Bias Monte Carlo (CBMC) simulations for elucidating the origins of thermodynamic non-idealities. The CBMC simulations reveal that two distinct regimes prevail during mixture adsorption. For low relative humidities less than say 20 %, the CO_2 loadings in the adsorbed phase is significantly higher than anticipated by the IAST. CBMC simulations of intermolecular distances for guest pairs reveal that failure of the IAST can be traced to the phenomenon of segregated adsorption. The H_2O-H_2O pairs are close together at typical distances of about 3 Å. The CO_2-H_2O pairs are typically 8 Å apart, occupying adjacent adsorption sites corresponding to the O atoms of the oxalate group. This implies that the CO_2 molecules face a less severe competitive adsorption with H_2O than is anticipated by the IAST, whose applicability mandates a uniform and homogeneous distribution of adsorbates in pore space. The situation changes dramatically at high values of relative humidities, typically larger than about 50 %; in this scenario, the adsorbed phase is significantly richer in H_2O. The CO_2 molecules are compelled to share same adsorption site with pairs of H_2O molecules that are hydrogen-bonded with each other. Consequently, the competition faced by CO_2 is significantly higher than anticipated by the IAST, resulting in significantly lower CO_2 uptakes.

The important message that emerges from this investigation is the need to incorporate the Real Adsorbed Solution Theory (RAST) for quantitative modelling of fixed-bed adsorbers in CO_2 capture with CALF-20.

1. Introduction

In current industrial practice, amine absorption technologies, that are energy intensive, are used for capture of CO_2 from a variety of gaseous mixtures. Potential reduction in the energy consumption is achievable by adsorption separations using fixed-bed adsorption devices [1–7]. For post-combustion CO_2 capture, 13X zeolite is considered to be the benchmark adsorbent, with the ability to meet the U.S. Department of Energy (US-DOE) targets for CO_2 purity and recovery [2].

Following the publication of Lin et al.[8], demonstrating the efficacy of Zinc-based Calgary Framework 20 (CALF-20) for CO_2 capture from humid flue gases, a number of complementary publications have explored a number of related and ancillary aspects [9–17]. Two publications [13,14] have presented comparisons of the experimental data on CO_2/H_2O mixture adsorption with the estimations of the Ideal Adsorbed Solution Theory (IAST). To set the scene, and define the objectives of this article, Fig. 1a presents the experimental data on component loadings for $CO_2(1)/H_2O(2)$ mixture adsorption in structured CALF-20 (80 % MOF:20 % polysulfone) at 295 K; these data have been backed-out from

* Corresponding author.
E-mail address: r.krishna@uva.nl (R. Krishna).

https://doi.org/10.1016/j.seppur.2024.128269
Received 14 April 2024; Received in revised form 23 May 2024; Accepted 2 June 2024
Available online 4 June 2024

Nomenclature

Latin alphabet

A	surface area per kg of framework, $m^2\ kg^{-1}$
c_i	molar concentration of species i, mol m^{-3}
c_{i0}	molar concentration of species i in fluid mixture at inlet to adsorber, mol m^{-3}
C	constant used in Eq. (7), kg mol^{-1}
f_i	partial fugacity of species i, Pa
L	length of packed bed adsorber, m
p_2^{sat}	saturation vapor pressure of water, Pa
P_i^0	sorption pressure, Pa
q_i	component molar loading of species i, mol kg^{-1}
$q_{sat,mix}$	saturation capacity of mixture, mol kg^{-1}
R	gas constant, 8.314 J mol^{-1} K^{-1}
$\%RH$	% relative humidity, dimensionless
t	time, s
T	absolute temperature, K
v	interstitial gas velocity in packed bed, m/s
x_i	mole fraction of species i in adsorbed phase, dimensionless
y_i	mole fraction of species i in the bulk gas mixture, dimensionless

Greek alphabet

γ_i	activity coefficient of component i in adsorbed phase, dimensionless
Λ_{ij}	Wilson parameters, dimensionless
θ	fractional pore occupancy, dimensionless
π	spreading pressure, N m
τ	dimensionless time $\tau \equiv vt/L$, dimensionless
Φ	surface potential, mol kg^{-1}

transient breakthrough experiments [8,12,13]. The dashed lines in Fig. 1a are estimations based on the Ideal Adsorbed Solution Theory (IAST) of Myers and Prausnitz [18]. The IAST estimates are in poor agreement with the experimental data. For $0 < \%RH < 40$, it is noteworthy that the H_2O loadings in the $CO_2(1)/H_2O(2)$ mixture are lower than both the unary H_2O loadings (indicated by solid blue line) and IAST estimates, prompting Lin et al.[8] to postulate the “suppression” of water sorption by CO_2.

Another way to demonstrate the non-idealities is to plot the mole fraction of CO_2 in the adsorbed phase mixture, x_1, as a function of the relative humidity; see Fig. 1b. We note that for $\%RH < 40; x_1 > 0.5$, the adsorbed phase mixture is richer in CO_2, i.e. significantly poorer in H_2O, than is anticipated by the IAST. On the other hand, for $\%RH > 40; x_1 < 0.5$, the adsorbed phase mixture is poorer in CO_2, i.e. richer in H_2O, than is anticipated by the IAST. None of the publications on CALF-20 have underscored the two different scenarios for failure of the IAST, nor offered any explanation for the possible reasons for its failure.

The IAST description of mixture adsorption equilibrium relies on a number of basic tenets [19–25]: (a) homogeneous distribution of guest adsorbates, (b) no preferential locations of any guest species within the pore landscape, and (c) adsorption enthalpies and surface areas of the adsorbed molecules do not change upon mixing with other guests. The occurrence of molecular clustering and hydrogen bonding should be expected to invalidate tenet (c) because the surface area occupied by a molecular cluster is different from that of each of the un-clustered guest molecules in the adsorbed phase. In a number of publications on CO_2 capture from mixtures containing N_2, CH_4, C_2H_4, C_2H_6, C_3H_8, and H_2O using cation-exchanged zeolites [2,19,21,23–29], the IAST has been shown to fail due to non-compliance with one or more of the aforementioned tenets.

The primary objective of this article is to elucidate the reasons for the distinct failure of the IAST, as evidenced in Fig. 1 for $CO_2(1)/H_2O(2)$ mixture adsorption in structured CALF-20.

Towards this end, Configurational-Bias Monte Carlo (CBMC) simulations for adsorption of CO_2/H_2O mixture adsorption in pristine CALF-20 crystals were undertaken. The simulation methodologies are the same as detailed in earlier publications [30–36]. The CALF-20 structure was considered to be rigid in the simulations. Recent works have included considerations of framework flexibility [16] and polymorphism [17]; both these aspects are ignored in the present work. The unit cell dimensions of CALF-20 crystals are $a = 8.9138$ Å; $b = 9.6935$ Å; $c = 9.4836$ Å with angles $\alpha = 90°$; $\beta = 115.895°$; $\gamma = 90°$; see pore landscape in Figure S3. The simulation box for conducting CBMC simulations consisted of $5 \times 3 \times 5 = 75$ unit cells. The interactions between adsorbed molecules are described with Lennard-Jones terms together with electrostatic interactions. For the atoms in the host metal organic framework (see Figure S4), the generic DREIDING [37] force fields were used. The framework atomic charges are from Gopalsamy et al.[9]; see Tables S2 and S3. CO_2 was described by a 3-site charged Lennard-Jones model as described by Garcia-Sánchez et al.[38]. Water is modeled using the four-site TIP4P-Ew potential [39]; TIP4P = 4-site transferable intermolecular potential (TIP4P) and Ew = Ewald technique. Further simulation details are provided in the Supplementary Material.

2. CBMC simulations

Fig. 2a presents the CBMC simulations conducted in this work for unary isotherms for $CO_2(1)$ and $H_2O(2)$ at 298 K. Fig. 2b shows CBMC simulations of component loadings, q_i, for $CO_2(1)/H_2O(2)$ mixture adsorption in CALF-20 at 298 K at a total fugacity = 15 kPa. The mole fraction of H_2O in the bulk gas mixture, y_2, is varied. In Fig. 2b, the loadings are plotted against $\%RH = \frac{f_2}{p_2^{sat}} \times 100$ where f_2 is the partial fugacity of water in the bulk gas phase, and p_2^{sat} is the saturation vapor pressure of water. At 298 K, p_2^{sat} is determined from the Antoine equation: $p_2^{sat} = 3150$ Pa. The dashed lines are the IAST estimations using the dual-site Langmuir-Freundlich model fits of the unary isotherms in Fig. 2a; the fit parameters as specified in Table S4. We note that the CO_2/H_2O binary mixture adsorption exhibits significant departures from thermodynamic idealities. For $\%RH < 25\%$, it is noteworthy is that the H_2O loading for mixture adsorption are lower than the corresponding IAST estimates, prompting Lin et al.[8] to postulate “suppression” of H_2O sorption by CO_2.

Another way to demonstrate the non-idealities is to plot the mole fraction of CO_2 in the adsorbed phase mixture, x_1, defined by

$$x_1 = \frac{q_i}{q_1 + q_2}; \quad x_2 = (1 - x_1) \tag{1}$$

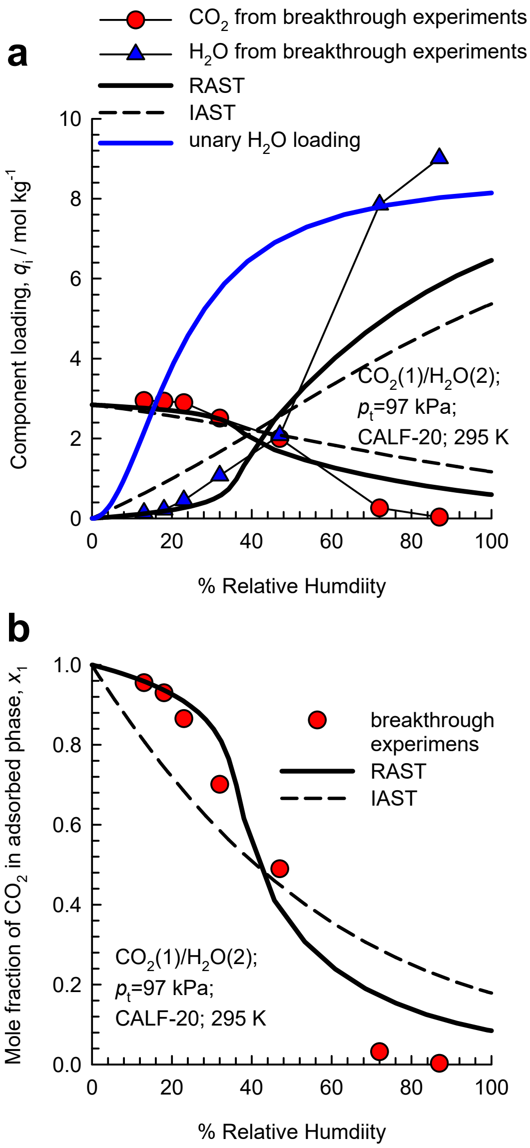

Fig. 1. (a) Experimental data of Lin et al.[8] (indicated by symbols) on component loadings for $CO_2(1)/H_2O(2)$ mixture adsorption in structured CALF-20 (80 % MOF:20 % polysulfone) at 295 K. The total pressure in the bulk gas phase is 97 kPa. In (a) the loadings are plotted against % relative humidity. (b) Plot of the mole fraction of CO_2 in the adsorbed phase mixture, x_1, as a function of the % relative humidity. The unary isotherm fits are provided in Table S1. The dashed and continuous lines are the IAST and RAST estimations, respectively. All calculation details, and input data are provided in the Supplementary Material accompanying this publication.

as a function of the relative humidity (Fig. 2c) and the mole fraction of H_2O in the bulk gas mixture (Fig. 2d). We also note that for $\%RH < 25\%$; $y_2 < 0.05$; $x_1 > 0.3$, the adsorbed phase mixture is richer in CO_2, i.e. poorer in H_2O, than is anticipated by the IAST. On the other hand, for $\%RH > 25\%$; $y_2 > 0.05$; $x_1 < 0.3$, the adsorbed phase mixture is poorer in CO_2 than is anticipated by the IAST. These two scenarios are precisely analogous to those witnessed in the experiments with the structured CALF-20 composite in Fig. 1b.

Additionally, CBMC simulations of component loadings, q_i, for $CO_2(1)/H_2O(2)$ mixture adsorption in CALF-20 at 298 K were determined for varying total fugacity f_t, maintaining the mole fraction of H_2O in the bulk gas mixture at a constant value $y_2 = f_2/f_t = 0.05$; see Fig. 3a. The dashed lines are the IAST estimations. Fig. 3b plots the mole fraction of CO_2 in the adsorbed phase mixture, x_1, as a function of $\%RH$. We again note that for this set of CBMC simulations, two different scenarios hold. For $\%RH < 10\%$; $x_1 > 0.5$, the adsorbed phase mixture is richer in CO_2 than is anticipated by the IAST. On the other hand, for $\%RH > 10\%$ $x_1 < 0.5$, the adsorbed phase mixture is poorer in CO_2, i.e. richer in H_2O, than is anticipated by the IAST.

To investigate the possibility of non-homogeneous distribution of adsorbate guests, CBMC simulation data on the spatial locations of the guest molecules were sampled to determine the inter-molecular distances; these distances are determined from the center of gravity of each guest molecule. By sampling a total of 10^6 simulation steps, the radial distribution function (RDF) were determined for CO_2-CO_2, CO_2-H_2O, and H_2O-H_2O separation distances. Fig. 4a,b presents the RDF data for guest pairs determined from CBMC simulations for $CO_2(1)/H_2O(2)$ mixture adsorption in CALF-20 at 298 K. The total fugacity in the bulk gas phase is 15 kPa with $y_2 = 0.04$; these conditions correspond to the first scenario in Fig. 2c,d: $\%RH < 25\%$; $y_2 < 0.05$; $x_1 > 0.3$. If we compare the first peaks, it is noteworthy that H_2O-H_2O pairs are close together at typical distances of about 3 Å. The CO_2-CO_2 pairs are typically 6.5 Å apart, occupying adjacent adsorption sites of CALF-20; these preferred sites correspond to the O atoms of the oxalate group; see also Figures S4 and S8. The CO_2-H_2O pairs are typically 8 Å apart, occupying adjacent adsorption sites. This implies that the CO_2 molecules face a less severe competitive adsorption with H_2O than is anticipated by the IAST. The segregated nature of adsorbate locations are visually observed in the computational snapshots in Fig. 4 and Figure S9. This explains the finding in Fig. 2c,d that for $y_2 < 0.05$, the adsorbed phase mixture is richer in CO_2 than is anticipated by the IAST; this is a direct consequence of the fact that CO_2 faces negligible competition with partner H_2O molecules.

Fig. 5a presents the data on RDF for center-to-center distances of CO_2-H_2O, and H_2O-H_2O pairs determined from CBMC simulations for adsorption of $CO_2(1)/H_2O(2)$ mixture adsorption in CALF-20 at 298 K; the total fugacity in the bulk gas phase is 15 kPa with $y_2 = 0.06$; these conditions correspond to the second scenario in Fig. 2c,d: $\%RH > 25\%$; $y_2 > 0.05$; $x_1 < 0.3$.We note that the first peaks for both CO_2-H_2O, and H_2O-H_2O pairs occurs at distances of about 3 Å. This implies that CO_2 faces stiffer competitive adsorption with partner H_2O molecules because of the preponderance of H_2O within the framework. Fig. 5b presents the data on RDF for O⋯H distances of CO_2-H_2O, and H_2O-H_2O pairs; strong hydrogen bonding manifests for H_2O-H_2O pairs. We note the first peak in the RDFs for H_2O-H_2O pairs occurs at a distance that is slightly less than 2 Å, that is characteristic of hydrogen bonding [40,41]. The computational snapshots in Fig. 5 and Figure S10 show that one CO_2 molecule is surrounded by two neighboring H_2O molecules that are hydrogen-bonded to each other. This implies that CO_2 faces enhanced competition with partner H_2O molecules that are H-bonded; such enhanced competition is not anticipated by the IAST that does not cater for formation of H-bonded molecular clusters.

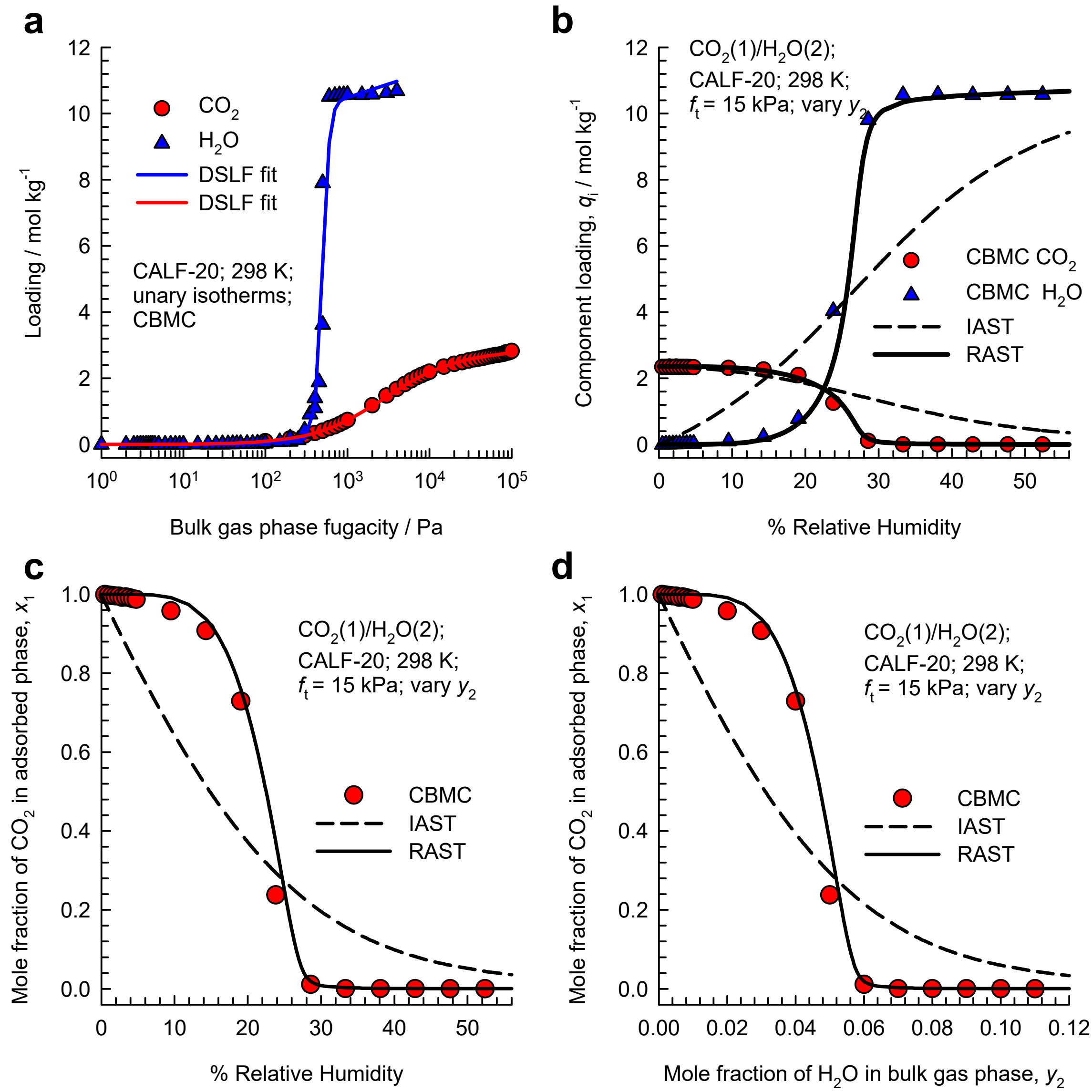

Fig. 2. (a) CBMC simulations for unary isotherms at 298 K, along with Dual-site Langmuir-Freundlich (DSLF) fits whose parameter values are provided in Table S4. (b) CBMC simulations of component loadings, q_i, for CO_2(1)/H_2O(2) mixture adsorption in CALF-20 at 298 K at a total fugacity $f_t = 15$ kPa, plotted as a function of $\%RH = \frac{f_2}{p_2^{sat}} \times 100$. The mole fraction of H_2O in the bulk gas mixture, $y_2 = f_2/f_t$, is varied. (c, d) Plot of the mole fraction of CO_2 in the adsorbed phase mixture, x_1, as a function of (c) $\%RH$, and (d) the mole fraction of H_2O in the bulk gas mixture. The dashed and continuous lines are the IAST and RAST estimations, respectively. All calculation details, and input data are provided in the Supplementary Material accompanying this publication.

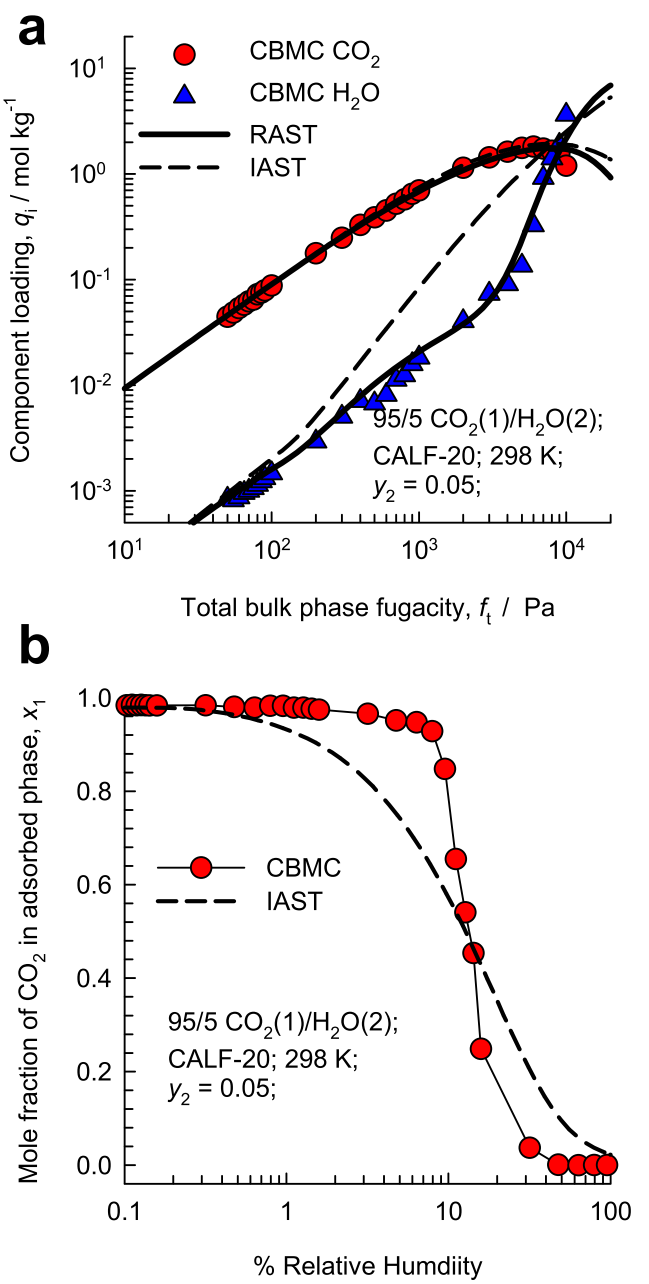

Fig. 3. (a) CBMC simulations of component loadings, q_i, for CO_2(1)/H_2O(2) mixture adsorption in CALF-20 at 298 K with varying total fugacity f_t, maintaining the mole fraction of H_2O in the bulk gas mixture at a constant value $y_2 = f_2/f_t = 0.05$. (b) Plot of the mole fraction of CO_2 in the adsorbed phase mixture, x_1, as a function of %RH. The dashed and continuous lines are the IAST and RAST estimations, respectively. All calculation details, and input data are provided in the Supplementary Material accompanying this publication.

3. The RAST for mixture adsorption equilibrium

For quantifying deviations from the IAST, we need to introduce activity coefficients [18,20,21,42–44]

$$f_i = P_i^0 \gamma_i x_i; \quad i = 1,2 \tag{2}$$

In eq (2), P_i^0 is the pressure for sorption of component i, which yields the same spreading pressure, π for each of the pure components, as that for the n-component mixture:

$$\frac{\pi A}{RT} \equiv \Phi = \int_0^{P_1^0} \frac{q_1^0(f)}{f} df = \int_0^{P_2^0} \frac{q_2^0(f)}{f} df \tag{3}$$

In eq (3), $q_i^0(f)$ is the *pure* component adsorption isotherm. The quantity A is the surface area per kg of framework, with units of m^2 per kg of the framework of the crystalline material; since the surface area A is not directly accessible from experimental data, the surface potential $\pi A/RT \equiv \Phi$, with the units mol kg^{-1}, serves as a convenient and practical proxy for the spreading pressure π [42,44–46].

The surface potential Φ is a measure of the pore occupancy. As derived in detail in Chapter 1 of the Supplementary Material, the fractional pore occupancy, θ, is related to the surface potential by

$$\theta = 1 - \exp\left(- \frac{\Phi}{q_{sat,mix}} \right) \tag{4}$$

where $q_{sat,mix}$ is the saturation capacity for mixture adsorption. Eq (4) implies that Φ may also be interpreted as a proxy for the pore occupancy. For values of Φ larger than about 30, the pores are nearly saturated, i.e. $\theta \approx 1$.

From the CBMC simulations of mixture adsorption, the activity coefficients in the adsorbed phase, can be calculated as detailed in Section 4.3 of the Supplementary Material. For the two sets of CBMC simulation data (presented in Fig. 2 and Fig. 3), the corresponding activity coefficients are plotted in Fig. 6a,b. Fig. 6a plots the activity coefficients as a function of the mole fraction of CO_2 in the adsorbed phase, x_1. The limiting values are

$$\gamma_i \to 1; \quad x_i \to 1 \tag{5}$$

Fig. 6b shows that the activity coefficients are also dependent on the surface potential, and must conform to the limiting behavior that both activity coefficients tend to unity at vanishingly small values of surface potential Φ

$$\Phi \to 0; \quad \gamma_1 \to 1; \quad \gamma_2 \to 1 \tag{6}$$

In view of Eq. (4), we may interpret Eq. (6) as requiring non-idealities to be of negligible importance at vanish pore occupancies, $\theta \to 0$. Models such as those of Wilson, Margules, and NRTL may be used for quantifying the dependence of the activity coefficients on the composition of the adsorbed mixture and the pore occupancy θ.

The continuous solid lines in Fig. 6 are calculations using the Wilson model

$$\begin{aligned} \ln(\gamma_1) &= \left(1 - \ln(x_1\Lambda_{11} + x_2\Lambda_{12}) - \frac{x_1\Lambda_{11}}{x_1\Lambda_{11} + x_2\Lambda_{12}} - \frac{x_2\Lambda_{21}}{x_2 + x_1\Lambda_{21}}\right)(1 - \exp(-C\Phi)) \\ \ln(\gamma_2) &= \left(1 - \ln(x_1\Lambda_{21} + x_2\Lambda_{22}) - \frac{x_1\Lambda_{12}}{x_1\Lambda_{11} + x_2\Lambda_{12}} - \frac{x_2\Lambda_{22}}{x_1\Lambda_{21} + x_2\Lambda_{22}}\right)(1 - \exp(-C\Phi)) \end{aligned} \tag{7}$$

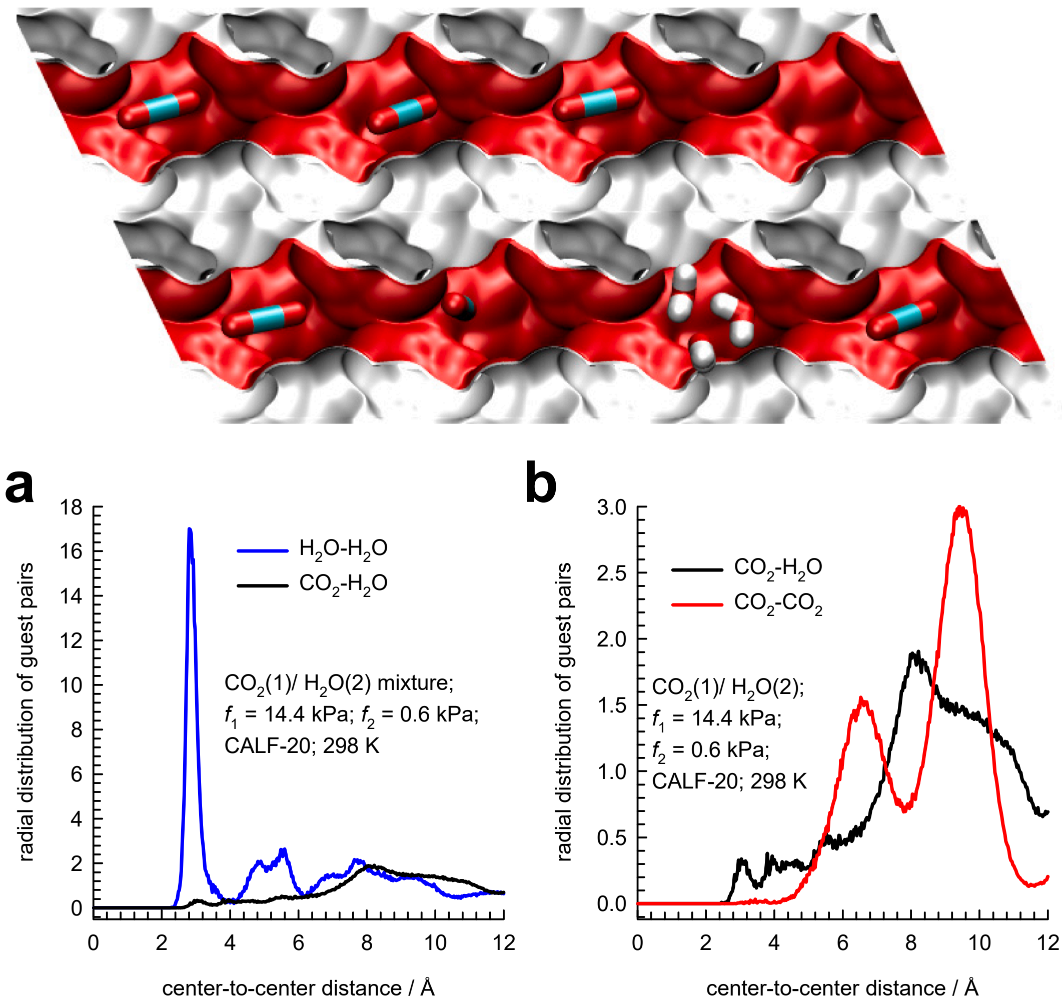

Fig. 4. (a, b) Radial Distribution Function (RDF) of center-to-center distances of CO_2-CO_2, CO_2-H_2O, and H_2O-H_2O pairs determined from CBMC simulations for adsorption of CO_2(1)/H_2O(2) mixture adsorption in CALF-20 at 298 K. The total fugacity in the bulk gas phase is 15 kPa with partial fugacities $f_1 = 14.4$ kPa, and $f_2 = 0.6$ kPa. The plotted RDF data has been normalized such that the area under each of the curves is identical to one another.

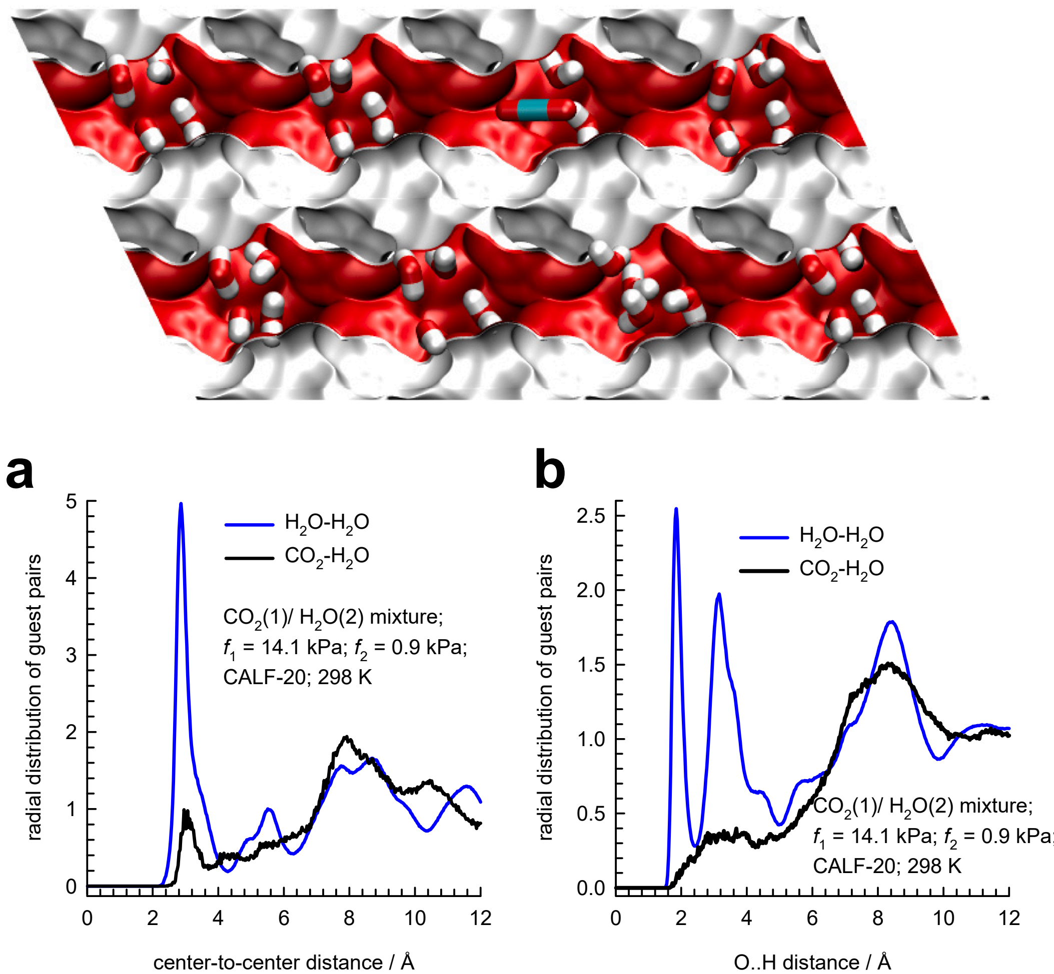

Fig. 5. Radial Distribution Function (RDF) of (a) center-to-center distances, and (b) O···H of CO_2-H_2O, and H_2O-H_2O pairs determined from CBMC simulations for adsorption of CO_2(1)/H_2O(2) mixture adsorption in CALF-20 at 298 K. The total fugacity in the bulk gas phase is 15 kPa with partial fugacities f_1 = 14.1 kPa, and f_2 = 0.9 kPa. The plotted RDF data has been normalized such that the area under each of the curves is identical to one another.

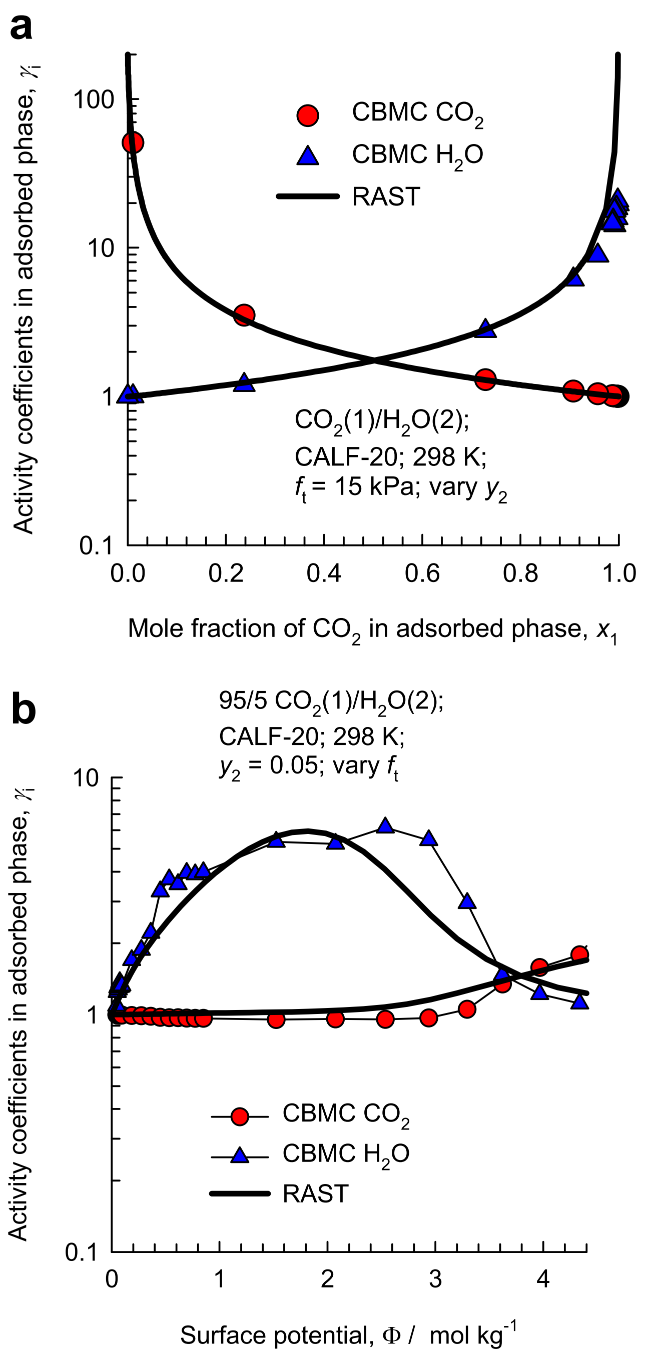

Fig. 6. (a) For the CBMC campaign in Fig. 2, plot of the activity coefficients in the adsorbed phase mixture, γ_i, as a function of the mole fraction of CO_2 in the adsorbed phase mixture, x_1, (b) For the CBMC campaign in Fig. 3, plot of the activity coefficients in the adsorbed phase mixture, γ_i, as a function of the surface potential Φ. The continuous solid lines are the RAST calculations; all calculation details, and input data are provided in the Supplementary Material accompanying this publication.

where in the values of the fitted Wilson parameters C; Λ_{12}; Λ_{21} are tabulated in Table S4. The inclusion of the correction factor $(1-\exp(-C\Phi))$ imparts the correct limiting behaviors for the activity coefficients in the Henry regime, as demanded by Eq. (6). We note, in passing, that this correction factor is often ignored in the RAST implementations in some published works [14,47–49]. The RAST calculations of the component loadings for the two sets of CBMC campaigns are indicated by the continuous solid lines in Fig. 2 and Fig. 3.

The RAST calculations for the component loadings for CO_2/H_2O mixture adsorption in structured CALF-20, determined from breakthrough experiments, are indicated by the continuous solid lines in Fig. 1a,b. For %RH = 73 %, and 87 %, the experimental H_2O loadings for mixture adsorption are in excess of the unary loadings; this characteristic cannot be modeled using the RAST. Noteworthily, RAST implementations of Kaur and Marshall [14], using either the NRTL or Margules models also experience similar limitations at the two highest values of %RH.

4. Transient breakthroughs in fixed-bed adsorber

Nguyen et al. [12] have presented experimental data on the influence of %RH on transient $CO_2(1)/H_2O(2)$ mixture breakthroughs in a laboratory scale fixed bed packed with structured CALF-20. We undertake modeling of these experiments using the simulation methodology as described in earlier works [4,50–52]. Fig. 7 compares breakthrough simulations using RAST (continuous colored lines) and IAST (dashed lines) for CO_2/H_2O mixtures with seven different values of %RH; the dimensionless concentrations, c_i/c_{i0} are plotted as function of the dimensionless time, $\tau \equiv vt/L$ where v is the interstitial gas velocity, and L is the length of the packed bed. Even a visual inspection reveals that there are two scenarios prevalent: (i) 32 % > %RH > 13 %, and (ii) 87 % > %RH > 32 %, corresponding to the two distinct scenarios as also underscored earlier in relation to Fig. 1b.

Fig. 8a,b present calculations of mole fraction of CO_2, and %RH of the gas mixture exiting the fixed bed determined from the breakthrough simulations with the RAST implementation. The comparisons with the corresponding experimental data presented in Figure 9a,b of Nguyen et al. [12] are provided in Figure S18. The agreement between simulations and experiment is good for %RH = 13, 18, 23, 32, 47. For %RH = 73 and 87, the agreement is poorer because at these high humidity values, the RAST fails to match equilibrated uptakes and adsorbed compositions; cf. Fig. 1a,b. In particular, the experimental H_2O uptakes for mixtures exceeds the unary uptake; this phenomenon cannot be modeled using the RAST.

The comparisons with the corresponding experimental data presented in Figure 9a,b of Nguyen et al. [12] are provided in Figure S18. The agreement between simulations and experiment is good for %RH = 13, 18, 23, 32, 47. For %RH = 73 and 87, the agreement is poorer because at these high humidity values, the RAST fails to match equilibrated uptakes and adsorbed compositions; cf. Fig. 1a,b. In particular, the experimental H_2O uptakes for mixtures exceeds the unary uptake; this phenomenon cannot be modeled using the RAST.

Fig. 8c,d present the corresponding calculations of mole fraction of CO_2, and %RH of the gas mixture exiting the fixed bed determined from the breakthrough simulations with the IAST implementation. Even a visual inspection of the IAST simulation results will lead us to conclude that these simulations do not reflect the experimental breakthroughs even in a qualitative manner.

5. Conclusions

Published experimental data [8,13] on $CO_2(1/H_2O(2)$ mixture adsorption in CALF-20 reveal strong thermodynamic non-idealities. The deviations from the IAST estimations follow two different scenarios, depending on the values of %RH. For low %RH values, the CO_2 adsorption is significantly stronger than anticipated by the IAST. For high %RH values, the CO_2 loadings in the adsorbed phase are significantly lower than anticipated by the IAST. CBMC simulations of $CO_2(1/H_2O(2)$ mixture adsorption in CALF-20 are used to elucidate the origins of thermodynamic non-idealities for these two different scenarios. Radial Distribution Functions (RDFs) of intermolecular distances of CO_2-CO_2, H_2O-H_2O, and CO_2-H_2O pairs reveal that failure of the IAST can be traced to the phenomenon of segregated adsorption prevails at low values of %RH. CO_2 locates at sites that are distant from H_2O; consequently, CO_2 faces less severe competition from H_2O than anticipated by the IAST, that mandates a homogeneous distribution of adsorbates within CALF-20 pores. For high values of %RH, the CO_2 molecules are compelled to share same

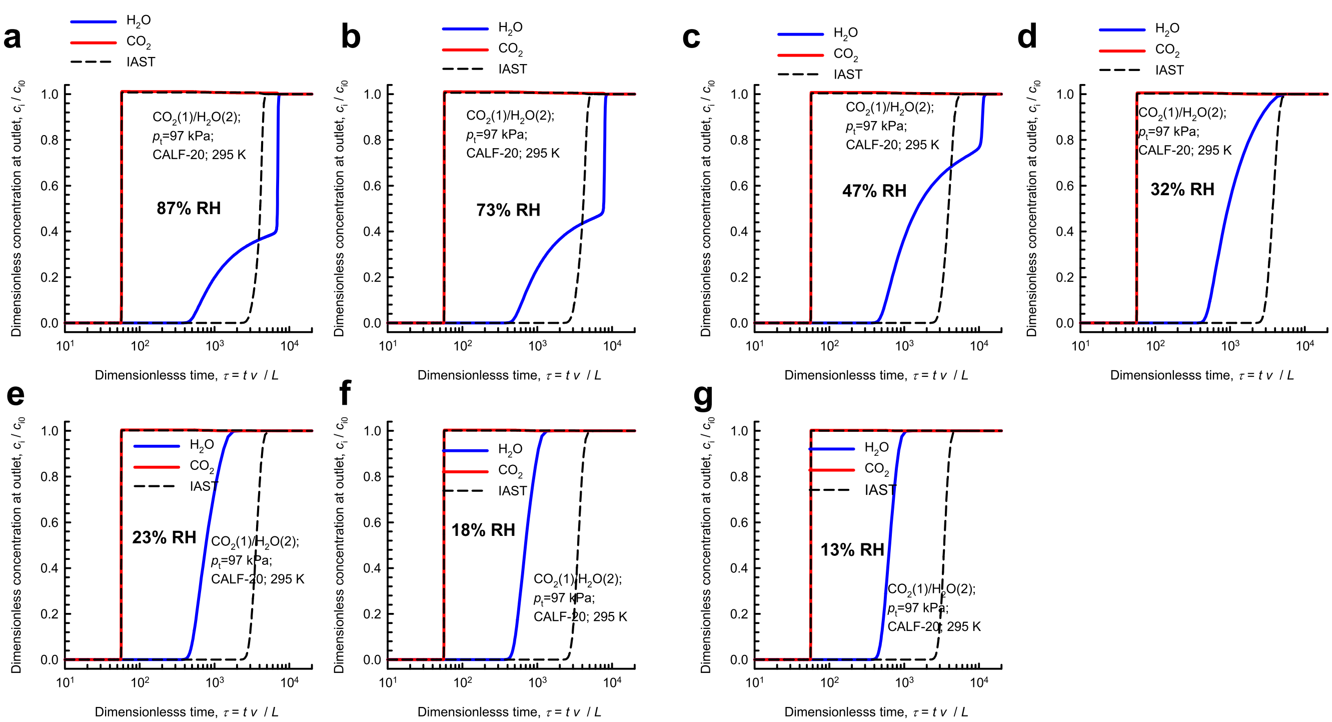

Fig. 7. Comparison of breakthrough simulations using RAST (continuous colored lines) and IAST (dashed lines) for CO_2/H_2O mixtures at a total pressure = 97 kPa, and temperature 295 K. Seven different values of %*RH* are considered. All calculation details, and input data are provided in the Supplementary Material accompanying this publication.

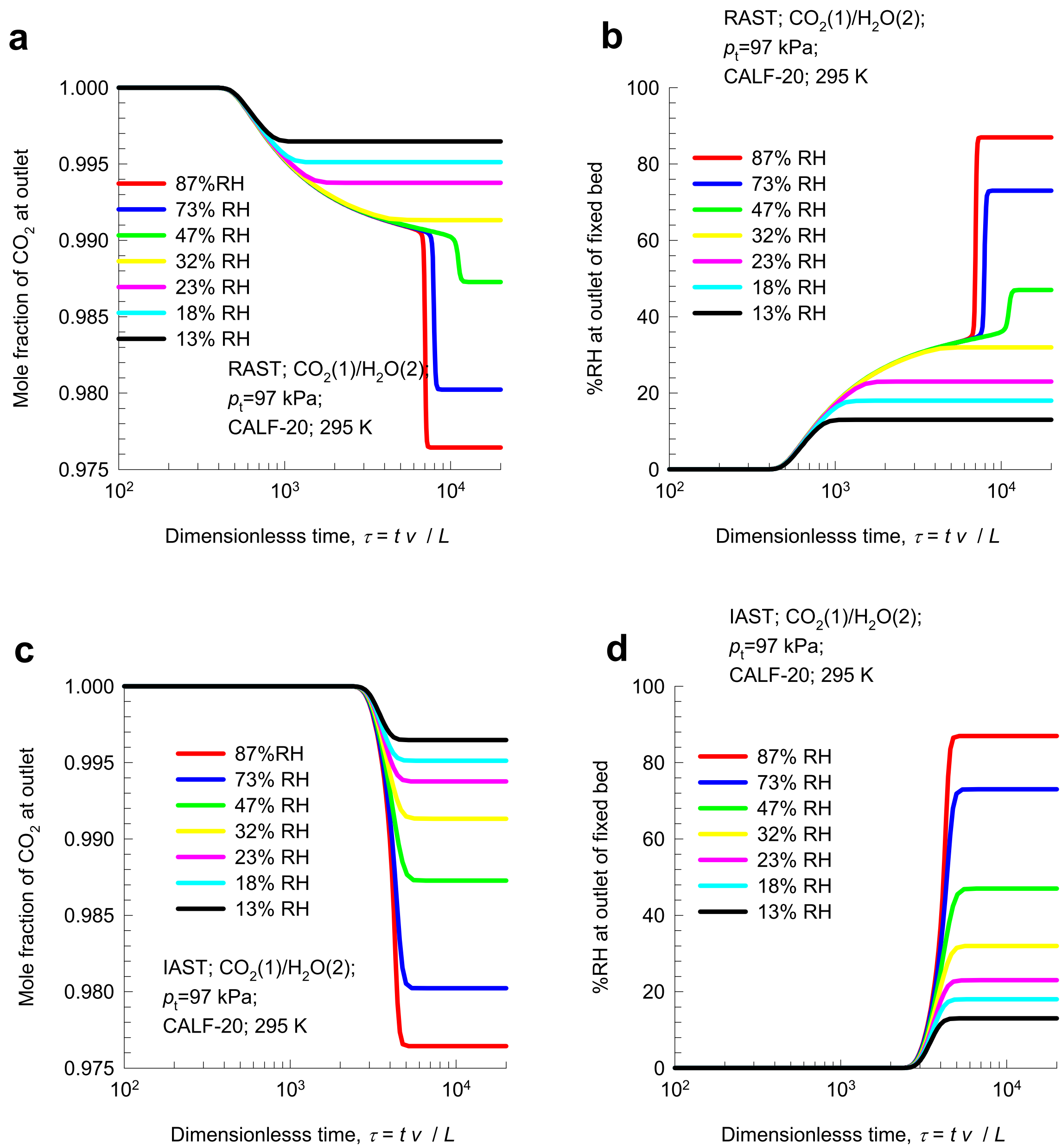

Fig. 8. Comparison of (a, c) mole fraction of CO_2, and (b, d) %*RH* of the gas mixture exiting the fixed bed determined from the breakthrough simulations using (a, b) RAST and (c, d) IAST. All calculation details, and input data are provided in the Supplementary Material accompanying this publication.

adsorption site with pairs of H_2O molecules that are hydrogen-bonded with each other. Consequently, the competition faced by CO_2 is significantly higher than anticipated by the IAST, resulting in significantly lower CO_2 uptakes. The IAST does not cater for molecular clustering resulting from hydrogen bonding between pairs of water molecules.

The modeling of thermodynamic non-idealities by introduction of activity coefficients needs to include the correction factor $(1-\exp(-C\Phi))$ in models such as the Wilson, Margules, or NRTL; this correction is of vital importance in order to ensure the proper limiting characteristics $\Phi\to 0$; $\gamma_1 \to 1$; $\gamma_2 \to 1$. Transient breakthrough simulations of CO_2/H_2O mixtures in fixed beds packed with CALF-20 are in good agreement with published breakthrough experimental data [12] provided the mixture adsorption equilibrium is appropriately described with the RAST model for mixture adsorption equilibrium.

CRediT authorship contribution statement

Rajamani Krishna: Writing – review & editing, Writing – original draft, Validation, Supervision, Methodology, Investigation, Conceptualization. **Jasper M. van Baten:** Molecular simulations, code development.

Declaration of competing interest

The authors declare that they have no known competing financial interests or personal relationships that could have appeared to influence the work reported in this paper.

Data availability

All data are provided in the Supplementary Material

Acknowledgement

The authors grateful acknowledge Dr. K. Gopalsamy and Prof G. Maurin for providing the atomic charges in CALF-20.

Appendix A. Supplementary material

Supplementary material to this article can be found online at https://doi.org/10.1016/j.seppur.2024.128269.

References

[1] G.D. Pirngruber, V. Carlier, D. Leinekugel-le-Cocq, Post-combustion CO_2 capture by vacuum swing adsorption using zeolites – a feasibility study, Oil Gas Sci. Technol. 69 (2014) 989–1003.
[2] N.S. Wilkins, A. Rajendran, Measurement of competitive CO_2 and N_2 adsorption on Zeolite 13X for post-combustion CO_2 capture, Adsorption 25 (2019) 115–133, https://doi.org/10.1007/s10450-018-00004-2.
[3] R. Krishna, J.M. van Baten, A comparison of the CO_2 capture characteristics of zeolites and metal-organic frameworks, Sep. Purif. Technol. 87 (2012) 120–126, https://doi.org/10.1016/j.seppur.2011.11.031.
[4] R. Krishna, Metrics for evaluation and screening of metal-organic frameworks for applications in mixture separations, ACS Omega 5 (2020) 16987–17004, https://doi.org/10.1021/acsomega.0c02218.
[5] D.M. Ruthven, S. Farooq, K.S. Knaebel, Pressure swing adsorption, VCH Publishers, New York, 1994.
[6] R. Krishna, Screening metal-organic frameworks for mixture separations in fixed-bed adsorbers using a combined selectivity/capacity metric, RSC Adv. 7 (2017) 35724–35737, https://doi.org/10.1039/C7RA07363A.
[7] R.T. Yang, Gas separation by adsorption processes, Butterworth, Boston, 1987.
[8] J.-B. Lin, T.T.T. Nguyen, R. Vaidhyanathan, J. Burner, J.M. Taylor, H. Durekova, F. Akhtar, R.K. Mah, O. Ghaffari-Nik, S. Marx, N. Fylstra, S.S. Iremonger, K. W. Dawson, P. Sarkar, P. Hovington, A. Rajendran, T.K. Woo, G.K.H. Shimizu, A scalable metal-organic framework as a durable physisorbent for carbon dioxide capture, Science 374 (2021) 1464–1469, https://doi.org/10.1126/science.abi7281.
[9] K. Gopalsamy, D. Fan, N. S, Y. Magnin, G. Maurin, Engineering of an Iso-reticular Series of CALF-20 MOF for CO_2 capture, ACS Appl. Eng. Mater. 2 (2024) 96–103, https://doi.org/10.1021/acsaenm.3c00622.
[10] C.-H. Ho, F. Paesani, Elucidating the competitive adsorption of H_2O and CO_2 in CALF-20: new insights for enhanced carbon capture metal−organic frameworks, ACS Appl. Mater. Interf. 15 (2023) 48287–48295, https://doi.org/10.1021/acsami.3c11092.
[11] Y. Magnin, E. Dirand, G. Maurin, P.L. Llewellyn, Abnormal CO_2 and H_2O diffusion in CALF-20(Zn) metal-organic framework: fundamental understanding of CO_2 capture, ACS Appl. Nano Mater. 6 (2023) 19963–19971, https://doi.org/10.1021/acsanm.3c03752.
[12] T.T.T. Nguyen, B.M. Balasubramaniam, N. Fylstra, R.P.S. Huynh, G.K.H. Shimizu, A. Rajendran, Competitive CO_2/H_2O adsorption on CALF-20, Ind. Eng. Chem. Res. 63 (2024) 3265–3281, https://doi.org/10.1021/acs.iecr.3c04266.
[13] T.T.T. Nguyen, Humid Post-Combustion CO_2 capture By Vacuum Swing Adsorption Using CALF-20, University of Alberta, Alberta, 2021. Ph.D. Thesis, Ph.D. Thesis,.
[14] H. Kaur, B.D. Marshall, Real adsorbed solution theory model for the adsorption of CO_2 from humid gas on CALF-20, ChemRxiv (2023) 1–18, https://doi.org/10.26434/chemrxiv-2023-2cp2c.
[15] A. Rajendran, G.K.H. Shimizu, T.K. Woo, The Challenge of water competition in physical adsorption of CO_2 by porous solids for carbon capture applications – a short perspective, Adv. Mater. 36 (2024) 2301730, https://doi.org/10.1002/adma.202301730.
[16] R. Oktavian, R. Goeminne, L.T. Glasby, P. Song, R. Huynh, O.T. Qazvini, O. Ghaffari-Nik, N. Masoumifard, J.L. Cordiner, P. Hovington, V. Van Speybroeck, P.Z. Moghadam, Gas adsorption and framework flexibility of CALF-20 explored via experiments and simulations, Nat. Commun. 15 (2024) 3898, https://doi.org/10.1038/s41467-024-48136-0.
[17] Z. Chen, C.-H. Ho, X. Wang, S.M. Vornholt, T.M. Rayder, T. Islamoglu, O.K. Farha, F. Paesani, K.W. Chapman, Humidity-responsive polymorphism in CALF-20: a resilient MOF physisorbent for CO_2 capture, ACS Mater. Lett. 5 (2023) 2942–2947, https://doi.org/10.1021/acsmaterialslett.3c00930.
[18] A.L. Myers, J.M. Prausnitz, Thermodynamics of mixed gas adsorption, A.I.Ch.E.J. 11 (1965) 121–130, https://doi.org/10.1002/aic.690110125.
[19] R. Krishna, J.M. van Baten, R. Baur, Highlighting the origins and consequences of thermodynamic nonidealities in mixture separations using zeolites and metal-organic frameworks, Microporous Mesoporous Mater. 267 (2018) 274–292, https://doi.org/10.1016/j.micromeso.2018.03.013.
[20] R. Krishna, J.M. van Baten, Fundamental Insights into the variety of factors that influence water/alcohol membrane permeation selectivity, J. Membr. Sci. 698 (2024) 122635, https://doi.org/10.1016/j.memsci.2024.122635.
[21] R. Krishna, J.M. Van Baten, How reliable is the ideal adsorbed solution theory for estimation of mixture separation selectivities in microporous crystalline adsorbents? ACS Omega 6 (2021) 15499–15513, https://doi.org/10.1021/acsomega.1c02136.
[22] R. Krishna, J.M. Van Baten, Water/alcohol mixture adsorption in hydrophobic materials: enhanced water ingress caused by hydrogen bonding, ACS Omega 5 (2020) 28393–28402, https://doi.org/10.1021/acsomega.0c04491.
[23] R. Krishna, J.M. Van Baten, Using molecular simulations for elucidation of thermodynamic non-idealities in adsorption of CO_2-containing mixtures in NaX zeolite, ACS Omega 5 (2020) 20535–20542, https://doi.org/10.1021/acsomega.0c02730.
[24] R. Krishna, J.M. Van Baten, Elucidation of selectivity reversals for binary mixture adsorption in microporous adsorbents, ACS Omega 5 (2020) 9031–9040, https://doi.org/10.1021/acsomega.0c01051.
[25] R. Krishna, J.M. Van Baten, Investigating the non-idealities in adsorption of CO_2-bearing mixtures in cation-exchanged zeolites, Sep. Purif. Technol. 206 (2018) 208–217, https://doi.org/10.1016/j.seppur.2018.06.009.
[26] M. Hefti, D. Marx, L. Joss, M. Mazzotti, Adsorption equilibrium of binary mixtures of carbon dioxide and nitrogen on zeolites ZSM-5 and 13X, Microporous Mesoporous Mater. 215 (2015) 215–228.
[27] I. van Zandvoort, E.-J. Ras, R. de Graaf, R. Krishna, Using transient breakthrough experiments for screening of adsorbents for separation of C_2H_4/CO_2 mixtures, Sep. Purif. Technol. 241 (2020) 116706, https://doi.org/10.1016/j.seppur.2020.116706.
[28] I. van Zandvoort, J.K. van der Waal, E.-J. Ras, R. de Graaf, R. Krishna, Highlighting non-idealities in C_2H_4/CO_2 mixture adsorption in 5A zeolite, Sep. Purif. Technol. 227 (2019) 115730, https://doi.org/10.1016/j.seppur.2019.115730.
[29] Y. Wang, M.D. LeVan, Adsorption equilibrium of binary mixtures of carbon dioxide and water vapor on zeolites 5A and 13X, J. Chem. Eng. Data 55 (2010) 3189–3195, https://doi.org/10.1021/je100053g.
[30] R. Krishna, J.M. van Baten, In silico screening of metal-organic frameworks in separation applications, Phys. Chem. Chem. Phys. 13 (2011) 10593–10616, https://doi.org/10.1039/C1CP20282K.
[31] R. Krishna, J.M. van Baten, In silico screening of zeolite membranes for CO_2 capture, J. Membr. Sci. 360 (2010) 323–333, https://doi.org/10.1016/j.memsci.2010.05.032.
[32] R. Krishna, J.M. van Baten, Describing mixture diffusion in microporous materials under conditions of pore saturation, J. Phys. Chem. C 114 (2010) 11557–11563.
[33] R. Krishna, J.M. van Baten, Diffusion of alkane mixtures in zeolites. validating the maxwell-stefan formulation using MD simulations, J. Phys. Chem. B 109 (2005) 6386–6396.
[34] R. Krishna, J.M. van Baten, Insights into diffusion of gases in zeolites gained from molecular dynamics simulations, Microporous Mesoporous Mater. 109 (2008) 91–108.
[35] R. Krishna, Describing the diffusion of guest molecules inside porous structures, J. Phys. Chem. C 113 (2009) 19756–19781, https://doi.org/10.1021/jp906879d.
[36] R. Krishna, Diffusion in porous crystalline materials, Chem. Soc. Rev. 41 (2012) 3099–3118, https://doi.org/10.1039/C2CS15284C.
[37] S.L. Mayo, B.D. Olafson, W.A. Goddard, DREIDING: a generic force field for molecular simulations, J. Phys. Chem. 94 (1990) 8897–8909.
[38] A. García-Sánchez, C.O. Ania, J.B. Parra, D. Dubbeldam, T.J.H. Vlugt, R. Krishna, S. Calero, Development of a transferable force field for carbon dioxide adsorption in zeolites, J. Phys. Chem. C 113 (2009) 8814–8820, https://doi.org/10.1021/jp810871f.
[39] H.W. Horn, W.C. Swope, J.W. Pitera, J.D. Madura, T.J. Dick, G.L. Hura, T. Head-Gordon, Development of an improved four-site water model for biomolecular simulations: TIP4P-Ew, J. Chem. Phys. 120 (2004) 9665, https://doi.org/10.1063/1.1683075.
[40] C. Zhang, X. Yang, Molecular dynamics simulation of ethanol/water mixtures for structure and diffusion properties, Fluid Phase Equilib. 231 (2005) 1–10.
[41] R. Krishna, J.M. van Baten, Hydrogen bonding effects in adsorption of water-alcohol mixtures in zeolites and the consequences for the characteristics of the maxwell-stefan diffusivities, Langmuir 26 (2010) 10854–10867, https://doi.org/10.1021/la100737c.
[42] O. Talu, A.L. Myers, Rigorous thermodynamic treatment of gas-adsorption, A.I.Ch.E.J. 34 (1988) 1887–1893.
[43] O. Talu, I. Zwiebel, Multicomponent adsorption equilibria of nonideal mixtures, A.I.Ch.E.J. 32 (1986) 1263–1276.
[44] F.R. Siperstein, A.L. Myers, Mixed-gas adsorption, A.I.Ch.E.J. 47 (2001) 1141–1159.
[45] R. Krishna, Thermodynamic insights into the characteristics of unary and mixture permeances in microporous membranes, ACS Omega 4 (2019) 9512–9521, https://doi.org/10.1021/acsomega.9b00907.
[46] R. Krishna, J.M. Van Baten, Using molecular simulations to unravel the benefits of characterizing mixture permeation in microporous membranes in terms of the spreading pressure, ACS Omega 5 (2020) 32769–32780, https://doi.org/10.1021/acsomega.0c05269.
[47] S. Sochard, N. Fernandes, J.-M. Reneaume, Modeling of adsorption isotherm of a binary mixture with real adsorbed solution theory and nonrandom two-liquid model, A.I.Ch.E.J. 56 (2010) 3109–3119.
[48] N. Mittal, P. Bai, I. Siepmann, P. Daoutidis, M. Tsapatsis, Bioethanol enrichment using zeolite membranes: molecular modeling, conceptual process design and techno-economic analysis, J. Membr. Sci. 540 (2017) 464–476.
[49] G. Calleja, A. Jimenez, J. Pau, L. Domínguez, P. Pérez, Multicomponent adsorption equilibrium of ethylene, propane, propylene and CO_2 on 13X zeolite, Gas Sep. Purif. 8 (1994) 247–256.
[50] R. Krishna, Highlighting the influence of thermodynamic coupling on kinetic separations with microporous crystalline materials, ACS Omega 4 (2019) 3409–3419, https://doi.org/10.1021/acsomega.8b03480.
[51] R. Krishna, Synergistic and antisynergistic intracrystalline diffusional influences on mixture separations in fixed bed adsorbers, Precis. Chem. 1 (2023) 83–93, https://doi.org/10.1021/prechem.2c00003.
[52] R. Krishna, Fundamental insights into intra-crystalline diffusional influences on mixture separations in fixed bed adsorbers, Chem. Bio. Eng. 1 (2024) 53–66, https://doi.org/10.1021/cbe.3c00057.